Dependence of powder neutron scattering on the dimensionality of magnetic order

1995 J. Phys.: Condens. Matter 7 6513

(http://iopscience.iop.org/0953-8984/7/32/017)

J. Phys.: Condens. Matter 7 (1995) 6513–6522. Printed in the UK

Dependence of powder neutron scattering on the dimensionality of magnetic order

W-H Li, W T Hsieh and K C Lee
Department of Physics, National Central University, Chung-Li 32054, Taiwan

Received 3 February 1995, in final form 20 April 1995

Abstract. The peak profiles of coherent scattering obtained in powder diffraction experiments that reflect the dimensionality of the ordered system are discussed. The well known expression that generates the powder diffraction pattern of a two-dimensionally ordered system is generalized to include couplings along the third dimension. Attention is concentrated on the magnetic systems, and the interactions between the adjacent layers are allowed to be either ferromagnetic or antiferromagnetic. A two-dimensionally ordered system gives Bragg peaks with characteristic sawtooth profiles at the $\{hk\}$ positions. As the correlations between the ordered layers develop, new Bragg peaks at the $\{khl\}$ positions appear and their widths are closely related to the correlation length along the third axis. A finite correlation length gives a width which is broader than the instrumental resolution, and its intrinsic width is inversely proportional to the correlation length. In the limit for long-range correlation along the third axis, symmetric peaks with their widths consistent with the instrumental resolution are then obtained. Neutron magnetic diffraction patterns taken at low temperatures on various high-T_c oxides are used as examples to illustrate the expression obtained.

1. Introduction

In layered compounds the interaction strength among the atoms within the layer (designed as the a–b plane) is usually much stronger than those along the third axis (designed as the c axis), i.e. $J_{ab} \gg J_c$, and they form quasi-two-dimensional systems. Two-dimensional (2D) phenomena can then be expected in the layered systems. However, the interactions along the c axis can still play a significant role in determining the basic properties of the layered systems. For instance, three-dimensional (3D) magnetic order can be induced by a finite J_c through a domain-enhancement effect in XY and Heisenberg systems even if $J_c \ll J_{ab}$. In a strictly 2D Ising system, where $J_c = 0$, 3D magnetic order is also induced (to minimize the total energy of the system) in such a way that it shows true long-range order at finite temperatures [1].

At the temperature for which the magnetic correlations in the a–b planes begin to develop, a quasi-2D magnetic system enters the 2D short-range ordered state that has a finite correlation length. As the temperature is reduced, when the correlation length in the plane reaches infinity, the system then is ordered two-dimensionally. The temperature at which the intraplane correlations reach infinity is the 2D ordering temperature of the system. If the couplings along the c axis are much weaker than those in the planes, the correlations along the c axis may still remain thermally random as the system orders two-dimensionally. However, once the ions in the planes are ordered, the couplings between the adjacent planes are then enhanced by domain population, which results in a rapid development of the correlations along the c axis. The system then enters an imperfect 3D ordered state in

0953-8984/95/326513+10$19.50

which it has a long-range correlation in the plane but a short-range correlation along the c axis. At even lower temperatures, the system eventually will order three-dimensionally with infinite correlation lengths along all three crystallographic directions. The temperature at which this occurs is the 3D ordering temperature of the system. The difference between the 2D and the 3D ordering temperatures is typically a few tenths of a degree, and it is usually difficult to observe this difference clearly [2,3]. Nevertheless, as more and more layered compounds with much weaker interplanar couplings are discovered, observation of the crossover from 2D to 3D character becomes feasible.

2D magnetic behaviour has been observed [4–10] in many of the high-T_c oxides by neutron diffraction, and the crossover from 2D to 3D magnetic character has been observed in several single-crystal samples [5,7]. If a powder sample is used, which consists of a collection of single crystals oriented randomly in all possible directions, the scattering must be averaged over all possible orientations of reciprocal space. In this study, we obtain an expression for the intensity distribution of the Bragg scattering from a powder sample, spanning the limiting cases from 2D short-range order to 3D long-range order. It clearly shows that the profile of the diffraction peaks depend strongly on the correlation length, and thus the dimensionality of the ordered system.

2. Theoretical considerations

In a purely 2D system the scattering from each of the ordered layers are completely uncorrelated, since the phase differences among the scattering amplitudes of the ordered layers are completely random [11]. The scattering plane of a 2D lattice thus consists of an ordered array of Bragg rods rather than Bragg points. Coherent scattering occurs whenever the wavevector change $\boldsymbol{Q} \equiv \boldsymbol{k}' - \boldsymbol{k}$, where $\boldsymbol{k}$ and $\boldsymbol{k}'$ are the incident and scattered wavevectors, respectively, lies on one of the scattering rods. When a powder sample is used, the scattering rods must then be averaged over all possible orientations which results in a very asymmetric form for the scattering characterized by a sharp leading edge on the small-Q side followed by a trailing edge extending to larger Q. In the scattering process, if Q is too small to reach a rod, then no coherent scattering occurs. As Q is increased, it will eventually exceed the minimum required to reach a rod. The scattering intensity abruptly increases as this occurs and then gradually decreases as Q is further increased until another rod farther out in reciprocal space is intersected and a second set of intensity peaks in. The powder diffraction peaks of a 2D system hence display a characteristic sawtooth shape [12–14].

As the layers are coupled together, the phase differences among the scattering amplitudes of the ordered layers are then coupled, and the scattering profile from the ordered layers gradually transforms from the 2D sawtooth form into symmetric lines. In the limit of long-range correlations along the c axis, the system becomes fully 3D. The uniform Bragg rods for the 2D system then renormalize into discrete Bragg points for a 3D system. Each of the three components of $\boldsymbol{Q}$ must now be restricted to specific values for observing Bragg scattering. An average over all possible orientations for powder samples then give rise to discrete spherical shells for scattering, and the projection of these shells onto the scattering plane yields a series of concentric circles. Discrete symmetric peaks with widths that are consistent with the instrumental resolution are therefore expected for Bragg scattering from 3D long-range ordered systems [15].

The scattering amplitudes of two magnetically coupled layers are different by a phase factor $C \exp(i\boldsymbol{Q} \cdot \boldsymbol{d})$, where $\boldsymbol{d}$ is the perpendicular component of the vector connecting the

two layers, and C is a constant describing the type of interplane coupling:

$$C = \begin{cases} +1 & \text{ferromagnetic coupling} \\ -1 & \text{antiferromagnetic coupling.} \end{cases}$$

The phase coupling among the ordered layers results in an undulation of the scattering intensity along the 2D rods and consequently a modulation in the diffraction profile. At a scattering angle 2θ, the intensity of the $\{hk\}$ magnetic reflection (characterized by wavevector $\boldsymbol{Q}$) from an N-layer coupled system is given as

$$I_{hk}(\theta) = \text{constant} \times M_{hk} \frac{|F_M(\boldsymbol{Q})|^2}{\sin\theta} S(\theta) \tag{1}$$

where M_{kk} is the multiplicity of the $\{hk\}$ reflection, and $F_M(\boldsymbol{Q})$ is the magnetic structure factor of the 2D magnetic unit cell which takes the form

$$F_M(\boldsymbol{Q}) = \sum_j [f_j(Q) \exp(-W_j) \exp(i\boldsymbol{Q} \cdot \boldsymbol{r}_j)] \hat{\boldsymbol{Q}} \times (\boldsymbol{M}_j \times \hat{\boldsymbol{Q}}) \tag{2}$$

where $f_j(Q)$ is the magnetic form factor which is Fourier transform of the atomic magnetization density of the jth ion, $\boldsymbol{M}_j$ is the thermal average of the magnetic moment on the jth ion located at $\boldsymbol{r}_j$, $\hat{\boldsymbol{Q}}$ is the unit vector along the direction of $\boldsymbol{Q}$, and the sum extends over all magnetic ions in the magnetic unit cell. At low temperatures the contribution from the Debye–Waller factor $\exp(-W_j)$, which accounts for the thermal vibration of the jth ion about its equilibrium position, is close to unity and can be neglected. $P(N)$ sums the phases of the N ordered layers according to

$$P(N) = 1 + C\exp(i\boldsymbol{Q} \cdot \boldsymbol{d}) + C^2 \exp(i\boldsymbol{Q} \cdot 2\boldsymbol{d}) + \cdots + C^{(N+1)} \exp(i\boldsymbol{Q} \cdot (N-1)\boldsymbol{d}) \tag{3}$$

so that the correlation length along the c axis is given by $L_c = (N-1)d$. The angular distribution of the scattering intensity is mainly controlled by the quantity $S(\theta)$ in equation (1), and it is given as

$$S(\theta) = \int_0^{\pi/2} \exp\left\{-\frac{4\pi L^2}{\lambda^2}[\sin\theta\cos\varphi - \sin\theta_{hk}]^2\right\} |P(N)|^2 \, d\varphi \tag{4}$$

where L is the correlation length of the magnetic ions that represents the characteristic size of the ordered domain of the layers, λ is the wavelength of the incident neutrons and θ_{hk} is the Bragg angle at which Q first intercepts the scattering rods. We note that

$$|P(N)|^2 = \frac{1 - 2C^N \cos[(4\pi Nd/\lambda)\sin\theta\sin\varphi] + C^{2N}}{1 - 2C\cos[(4\pi d/\lambda)\sin\theta\sin\varphi] + C^2}. \tag{5}$$

In a 2θ scan, one experimentally scans the instrumental resolution over the intrinsic scattering lines. The observed angular variation in the intensity hence has the form of the instrumental resolution function convoluted with the intrinsic profile, i.e.

$$I_{obs}(\theta, W) = \int_0^{\pi} I_{hk}(\theta') R(\theta' - \theta, W) \, d\theta' \tag{6}$$

where $R(\theta' - \theta, W)$ is the instrumental resolution function of width W and centred at θ. We note that the instrumental resolution of a neutron diffractometer may be well approximated by a Gaussian function, and its width is determined by the collimation and monochromating crystal used [16].

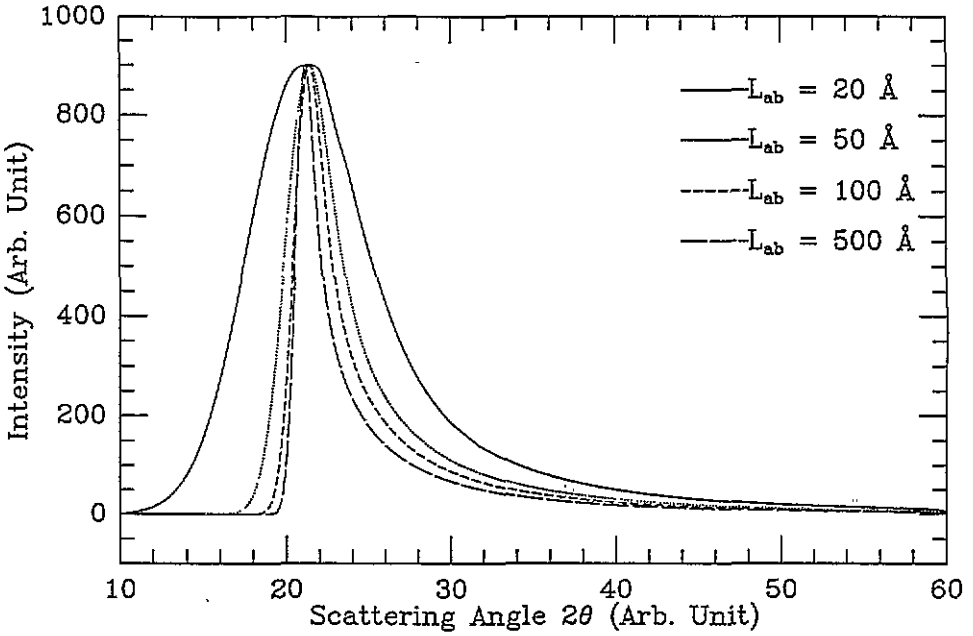

Figure 1. Intensity versus scattering angle calculated for the $\{\frac{1}{2}\frac{1}{2}\}$ wavevector using $N = 1$ and correlation lengths of $L = 20$, 50, 100 and 500 Å. The width of the peak depends strongly on L and the peak position displaced from $2\theta_{hk}$ towards a larger scattering angle for small values of L.

3. Diffraction by 2D lattices

Figure 1 shows the calculated $\{\frac{1}{2}\frac{1}{2}\}$ powder diffraction pattern of a 2D antiferromagnetically ordered system. The curve was calculated according to equations (1)–(6) using $N = 1$, $L = 20, 50, 100$ and 500 Å and a Gaussian instrumental resolution of 1° full width at half-maximum (FWHM), which is typical for a neutron diffraction set-up. The intensity abruptly increases as the scattering angle 2θ exceeds the minimum required for $Q = (4\pi \sin\theta)/\lambda$ to reach the $\{\frac{1}{2}\frac{1}{2}\}$ scattering rod; it then gradually and monotonically decreases as 2θ is increased further. The peak profiles among the curves shown are substantially different. It is clear that the widths of the diffraction peaks depend strongly on the correlation length and, the shorter the correlation length, the broader is the peak width. However, the widths for the curves calculated with $L > 500$ Å are very close to the instrumental resolution, and they become difficult to distinguish. Moreover, the peak position is also shifted to a larger scattering angle for finite correlations, and this displacement of the peak position can be quite large for small values of L. If the 2D character of the reflections was not realized and the peaks were treated as 3D powder lines, erroneous conclusions on the lattice constants could be easily drawn.

The Bragg reflections originating from the magnetic ordering of the Tb ions in $Pb_2Sr_2TbCu_2O_8$ serve as a good example of 2D short-range lattice reflections. The Tb atoms in $Pb_2Sr_2TbCu_3O_8$ form an orthorhombic unit cell, where the distance between the nearest neighbours along the c axis is more than four times that in the a–b plane [17]. The crystallographic anisotropy leads to highly anisotropic magnetic interactions, which results in a 2D magnetic character. Significant magnetic correlations were found [7] to develop

below $T \simeq 10$ K with the correlation length increasing with decreasing temperature, and 2D long-range order develops at $T_N = 5.3$ K. Figure 2 shows the magnetic Bragg reflection obtained from polycrystalline $Pb_2Sr_2TbCu_3O_8$ at $T = 6.5$ K, which is above the ordering temperature. The data were obtained using neutrons with $\lambda = 4.21$ Å, and the index shown is based on the Tb chemical unit cell. The magnetic signal shown in figure 2 was isolated from the nuclear signal by subtracting the data collected at $T = 20$ K from the data taken at $T = 6.5$ K. Note that this is the classic profile of a 2D short-range correlation. The solid curve shown in figure 2 is a fit of the data to equations (1)–(6) for the $\{\frac{1}{2}\frac{1}{2}\}$ wavevector, and the correlation length obtained from the fit is $L = 150$ Å. At temperatures below 5.3 K the system orders two-dimensionally with the nearest-neighbour spins of the Tb ions aligned antiparallel as shown in the inset of figure 2.

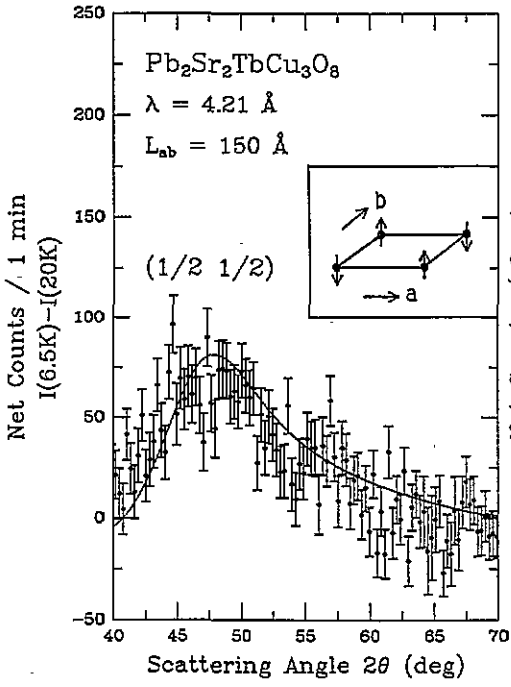

Figure 2. Angular scan through the magnetic scattering of $Pb_2Sr_2TbCu_3O_8$ at $T = 6.5$ K. The solid curve is a fit to the theoretical curve for the $\{\frac{1}{2}\frac{1}{2}\}$ wavevector, and the correlation length thus obtained is 150 Å. The inset shows the spin configuration of the Tb ions at low temperatures.

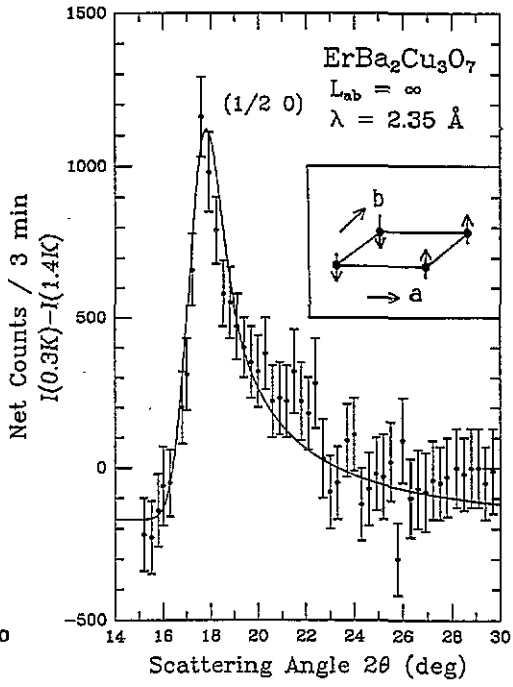

Figure 3. Magnetic scattering intensity observed in $ErBa_2Cu_3O_7$ at $T = 0.33$ K. The width of the peak is consistent with the instrument resolution, indicating long-range order for the Er spins. The solid curve is the theoretical scattering profile expected for a 2D long-range-ordered system. The inset shows the spin structure of the Er ions at low temperatures.

As an example of Bragg scattering from a 2D long-range ordered system, figure 3 shows the magnetic reflection obtained from polycrystalline $ErBa_2Cu_3O_7$ at $T = 0.33$ K, which is below the ordering temperature of the Er spins [18]. The asymmetric sawtooth profile with a width that is consistent with the instrumental resolution is a classic profile of a 2D long-range ordered system. The data were obtained using neutrons with $\lambda = 2.352$ Å, and on the basis of the Er chemical unit cell the peak may be indexed as the $\{\frac{1}{2}0\}$ reflection. The solid curve through the data in figure 3 is a fit of the data to equations (1)–(6) for the

$\{\frac{1}{2}0\}$ wavevector using $N = 1$ and $L = \infty$. This result indicates that at $T = 0.33$ K the Er spins order two-dimensionally with an infinite correlation length. The Er spins form chains along the b axis with spins pointing in the same direction, while the adjacent chains along the a axis are antiparallel. The spin configuration is shown in the inset of figure 3.

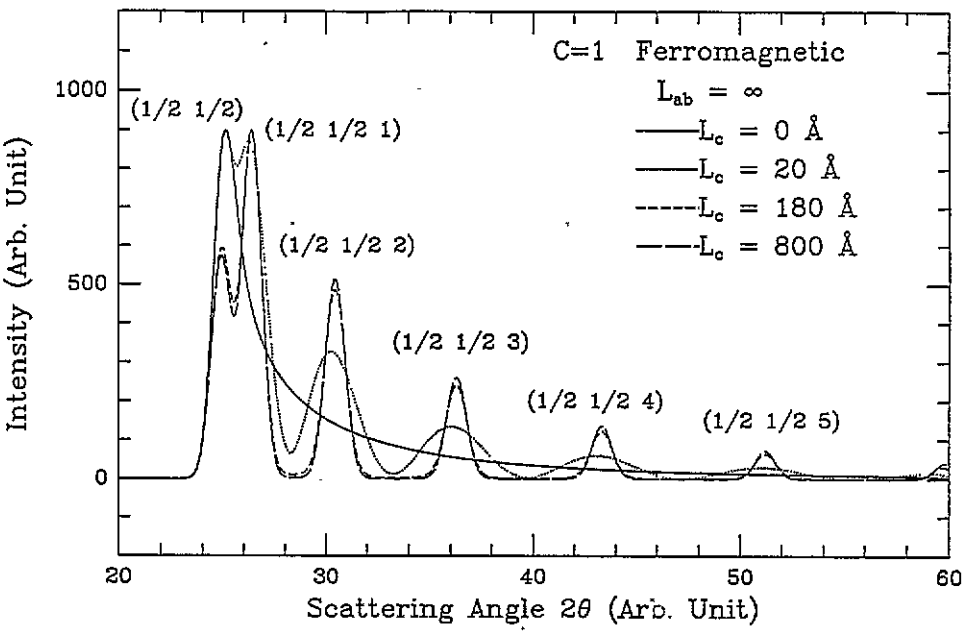

Figure 4. The calculated powder pattern for systems with ferromagnetic ($C = 1$) interplane coupling. New peaks at the $\{\frac{1}{2}\frac{1}{2}l\}$ (where l is an integer) positions appeared. As the correlation length along the c axis is increased, the peaks become more symmetric and their widths narrower.

4. Diffraction by 3D lattices

Figure 4 shows the dependence of the diffraction profile on the correlation length along the c axis, where antiferromagnetic long-range intraplane coupling ($L = \infty$) and ferromagnetic short-range interplane coupling ($C = 1$ and $N =$ finite) with moments pointed along the c axis were assumed. The curves were calculated according to equations (1)–(6) convoluted with a Gaussian instrumental resolution of 1° FWHM. As the interplane coupling develops, the 2D sawtooth profile renormalizes into more symmetric peaks and new peaks at the $\{\frac{1}{2}\frac{1}{2}l\}$ (where l is an integer) positions appeared, and the $\{\frac{1}{2}\frac{1}{2}\}$ reflection should now be indexed as the $\{\frac{1}{2}\frac{1}{2}0\}$ reflection. An integer for the third Miller index means that the magnetic unit cell is the same as the nuclear unit cell along that axis. This is as expected, since the coupling along the c axis is chosen to be ferromagnetic. As the correlation length along the c axis is increased, the peaks become more symmetric and their widths narrower.

If the interplane coupling is antiferromagnetic ($C = -1$), the $\{\frac{1}{2}\frac{1}{2}\}$ reflection 'shifted' to the $\{\frac{1}{2}\frac{1}{2}\frac{1}{2}\}$ position and new peaks at the $\{\frac{1}{2}\frac{1}{2}\frac{l}{2}\}$ rather than the $\{\frac{1}{2}\frac{1}{2}l\}$ positions appear as the interplane coupling develops. Figure 5 shows the calculated diffraction profiles for the

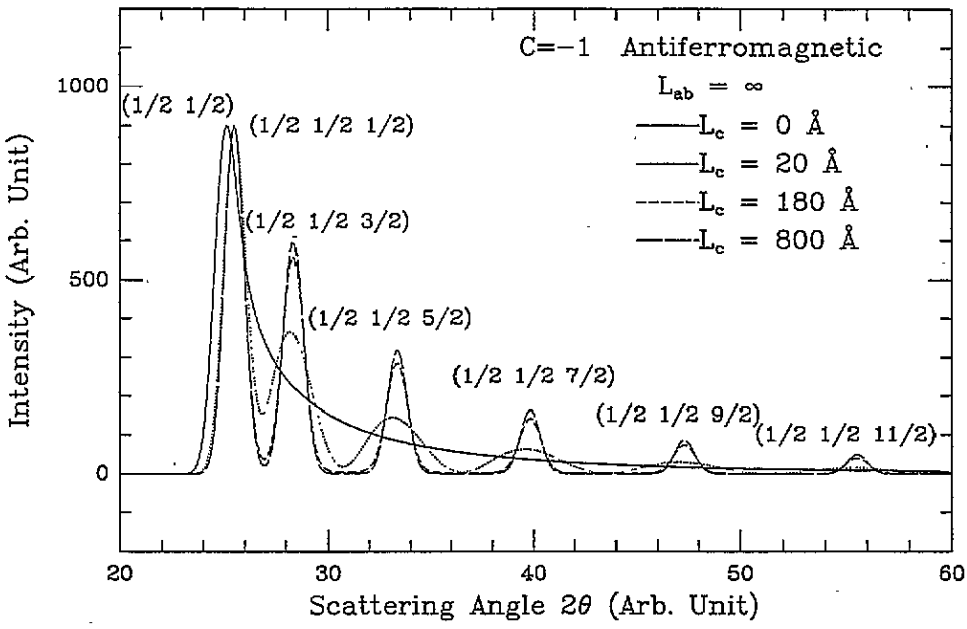

Figure 5. The calculated powder pattern for systems with antiferromagnetic ($C = -1$) interplane coupling. The 3D peaks now appear at the $\{\frac{1}{2}\frac{1}{2}\frac{l}{2}\}$ positions; this reflects the fact that the magnetic unit cell double the nuclear unit cell along all three crystallographic directions.

cases of antiferromagnetic coupling along all three axes where different correlation lengths along the c axis were used. The appearance of the $\{\frac{1}{2}\frac{1}{2}\frac{l}{2}\}$ peaks reflects the fact that the magnetic unit cell is now doubled along all three crystallographic directions relative to the nuclear unit cell. Figures 4 and 5 clearly indicate that diffraction profiles depend strongly on the correlation length, and such figures can be used to determine the correlation length from the observed diffraction pattern.

The superconducting properties of most of the high-T_c oxides were found to be not affected by the magnetic ordering of the rare-earth ions at low temperatures. The rare-earth sublattice is therefore believed to be electronically decoupled from the superconducting copper–oxygen sublattice [19]. One exception to this behaviour occurs in Pr compounds. It is now generally believed that the Pr ions are strongly coupled along the c axis through the copper–oxygen layers located between them [20–22]. The Tb ions in $Pb_2Sr_2TbCu_3O_8$ order at $T_N = 5.3$ K; nevertheless even at $T = 1.36$ K the scattering observed [7] is still 2D. The coupling of the Pr ions in $Pb_2Sr_2PrCu_3O_8$ is expected to be stronger than that of Tb ions in $Pb_2Sr_2TbCu_3O_8$. The $Pb_2Sr_2PrCu_2O_8$ system is then a better candidate for observing the imperfect 3D diffraction originating from the magnetic ordering of the Pr ions. Figure 7 shows the magnetic diffraction pattern obtained from $Pb_2Sr_2PrCu_3O_8$ at $T = 1.36$ K, which is well below $T_N \approx 7$ K [23], using neutrons with $\lambda = 2.352$ Å. The widths of the observed magnetic peaks are much broader than the 1° expected for the instrumental resolution. The solid curve shown in figure 6 is a fit of the data to equations (1)–(6) assuming long-range order in the a–b plane ($L = \infty$), short-range correlations ($N = 2$) along the c axis, and a moment pointed along the c axis. The indices shown are based on the Pr chemical unit cell, and the underlying spin structure of Pr hence consists of nearest-neighbour spins that are aligned antiparallel along all three crystallographic directions as shown in the inset of

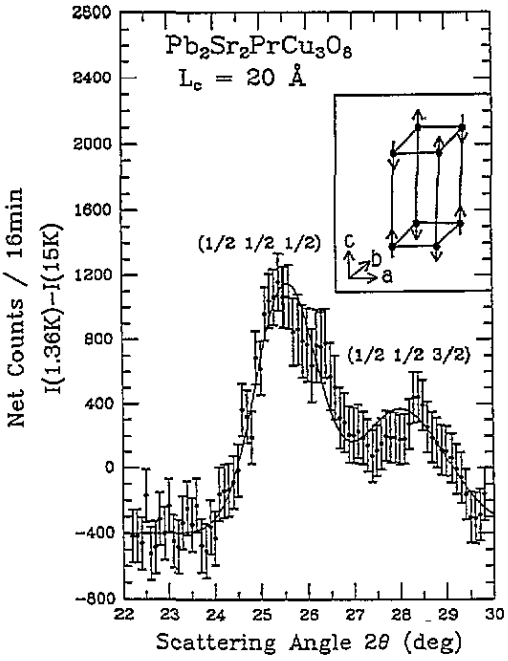

Figure 6. Magnetic scattering intensity observed in $Pb_2Sr_2PrCu_3O_8$ at $T = 1.36$ K. The solid curve is a fit to the theoretical curve with $L = \infty$ and $N = 2$, which corresponds to a long-range order within the layer and a short-range order along the c axis. The inset shows the spin structure of the Pr ions in $Pb_2Sr_2PrCu_3O_8$.

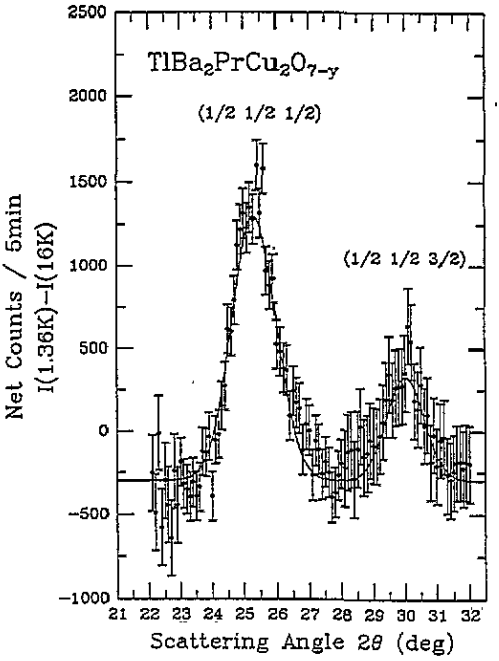

Figure 7. The difference between the diffraction patterns taken from $TlBa_2PrCu_2O_7$ at $T = 1.36$ K and $T = 16$ K, where the indexed $\{\frac{1}{2}\frac{1}{2}\frac{1}{2}\}$ and $\{\frac{1}{2}\frac{1}{2}\frac{3}{2}\}$ reflections are the magnetic intensities that develop at low temperatures. The solid curve is a fit to the theoretical curve with $N = \infty$ and $L = \infty$, which corresponds to 3D long-range order.

figure 6.

Although the rare-earth magnetism of the high-T_c oxides is in general believed to be 2D in nature, 3D ordering has also been observed in many of the layered cuprates. One example of 3D behaviour is the Pr ordering observed [24] in the single-Tl-layer compound $TlBa_2PrCu_2O_7$ [25]. Figure 7 shows the difference between the diffraction patterns taken at $T = 1.36$ K and $T = 16$ K using neutrons with $\lambda = 2.352$ Å, where the indexed $\{\frac{1}{2}\frac{1}{2}\frac{1}{2}\}$ and $\{\frac{1}{2}\frac{1}{2}\frac{3}{2}\}$ Bragg reflections are the magnetic intensities that develop at low temperatures. The widths of the observed peaks are at the instrumental resolution limit which suggests 3D long-range order of the Pr spins. The solid curve is a fit of the data to equations (1)–(6) with $N = \infty$ and $L = \infty$, i.e. assuming long-range order along all three crystallographic directions, and the moment directed along the c axis. All three Miller indices are half-integers showing that the nearest-neighbour Pr spins are aligned antiparallel along all three crystallographic directions.

5. Conclusions

We have obtained an expression that generates the diffraction profiles of ordered systems. There are in total five parameters included in the expression. Among them L, the correlation length within the 2D layers, and N, the number of layers that are coupled, control the

dimensionality of the ordered state. In the case of $N = 0$ and $L =$ finite, the expression gives asymmetric diffraction profiles that describe 2D short-range order. If the correlations within the layers are extended to infinity, i.e. $N = 0$ and $L = \infty$, sawtooth diffraction profiles that describe 2D long-range order are then obtained. As the correlations among the layers develop, i.e. $N =$ finite and $L = \infty$, symmetric diffraction peaks with widths that are broader than the instrumental resolution are obtained for imperfect 3D order. In the limit of $N = \infty$ and $L = \infty$, symmetric diffraction peaks with widths that are consistent with the instrumental resolution are obtained for 3D long-range order. Thus, the expression covers the full range from 2D short-range order to 3D long-range order. It is particularly useful in studying the effect of temperature on the development of the correlations among ions.

The types of interaction between the ions are specified using two parameters: M_j and C representing the intraplane and interplane coupling, respectively. The spin direction of the jth ions located in the planes is specified by the direction of M_j, which is the thermal average of the magnetic moment on the jth ion. On the other hand, scattering of neutrons by a spin-up ion has a phase difference of π from that of a spin-down ion. Ferromagnetic and antiferromagnetic coupling between the adjacent layers are hence specified by $C = 1$ and $C = -1$, respectively. The fifth parameter θ_{hk}, which is the Bragg angle for Q first intercepts the scattering rods, gives the 2D peak position and is determined from the intraplane lattice constants.

Although we have used neutron magnetic Bragg reflection data obtained from the rare-earth ordering in high-T_c layered cuprates as examples to examine the expression obtained, this does not necessarily restrict its application to neutron diffraction data. If, for example, x-ray diffraction data were used, the appropriate resolution function in equation (6) can be chosen consistent with the x-ray instrument used. Also, if the basic interactions under study are not magnetic in nature, the structure factor in equation (2) should be modified consistent with the type of interaction under investigation. We finally note that powder diffraction profiles from a 2D system show evidence of the 2D character in the form of an asymmetric lineshape, where only the magnitude of the reciprocal-lattice vector can be identified. Ideally one would like to make measurements on single-crystal samples, where rods of scattering are directly observed and reciprocal-lattice vectors can then be uniquely defined.

Acknowledgments

The research at NCU was supported by the National Science Council of the Republic of China under grant NSC 84-2112-M-008-022 and was partially supported by the Nuclear Energy Council under grant 842001-INER01*.

References

[1] White R M and Geballe T H 1979 *Long Range Order in Solids* (London: Academic)
[2] Bertaut E E 1950 *Acta Crystallogr.* **3** 14
[3] Steiner M, Villain J and Windsor C G 1970 *Adv. Phys.* **25** 87
[4] Dirken M W and de Jongh L J 1987 *Solid State Commun.* **64** 1201
[5] Lynn J W, Clinton T W, Li W-H, Erwin R W, Liu J Z, Vandervoort K and Shelton R N 1989 *Phys. Rev. Lett.* **63** 2606
[6] Zhang H, Lynn J W, Li W-H, Clinton T W and Morris D E 1990 *Phys. Rev.* B **41** 11 229

[7] Clinton T W, Lynn J W, Liu J Z, Jia Y X and Shelton R N 1991 *J. Appl. Phys.* **70** 5751
[8] Guillaume M, Fischer P, Roessli B, Podlesnyak A, Schefer J and Furrer A *1993 Solid State Commun.* **88** 57
[9] Wu S Y, Hsieh W T, Li W-H, Lee K C, Lynn J W and Yang H D 1994 *J. Appl. Phys.* **75** 6598
[10] Clinton T W 1992 *PhD Thesis* University of Maryland, College Park
[11] Razafitianamaharavo A 1989 *J. Physique* **50** 3133
[12] Warren B E 1941 *Phys. Rev.* **59** 693
[13] Kjems J K, Passell L, Taub H, Dash J G and Novaco A D 1976 *Phys. Rev.* B **13** 1446
[14] Zhang H, Lynn J W and Morris D E 1992 *Phys. Rev.* B **45** 10002
[15] Bacon G E 1975 *Neutron Diffraction* 3rd edn (Oxford: Clarendon)
[16] Cooper M J and Nathana R 1968 *Acta Crystallogr.* A **24** 619
[17] Cava R J, Batlogg B, Krajewski J J, Rupp L W, Schneemeyer T, Siegrist T, van Dover R B, Marsh P, Peck W F Jr, Gallagher P K, Glarum S H, Marshall J H, Farrow R C, Waszczak J V, Hull R and Trevor P 1988 *Nature* **336** 211
[18] Lynn J W, Li W-H, Li Q, Ku H C, Yang H D and Shelton R N 1987 *Phys. Rev.* B **36** 2374
[19] See, for example,
Lynn J W (ed) 1990 *High Temperature Superconductivity* (New York: Springer)
[20] Xiao G, Cieplak Z, Garvin A, Streitz F H, Bakhshai A and Chien C L 1988 *Phys. Rev. Lett.* **60** 1446
[21] Li W-H, Lynn J W, Shanthakumar S, Clinton T W, Kebede A, Jee C-S, Crow J E and Mihalisin T 1989 *Phys. Rev.* B **40** 5300
[22] Phillips N E, Fisher R A, Caspary R, Amato A, Radousky H B, Peng J L, Zhang L and Shelton R N 1991 *Phys. Rev.* B **43** 11488
[23] Hsieh W T, Li W-H, Lee K C, Lynn J W, Shieh J H and Ku H C 1994 *J. Appl. Phys.* **76** 7124
[24] Hsieh W T, Chang K J, Li W-H, Lee K C, Lynn J W, Lai C C and Ku H C 1994 *Phys. Rev.* B **49** 12200
[25] Manako T, Shimakawa Y, Kubo Y, Satoh T and Igarashi H 1988 *Physica* C **156** 315